Protection and Control of
Modern Power Systems

ORIGINAL RESEARCH

Open Access

Strategies for improving resilience of regional integrated energy systems in the prevention–resistance phase of integration

Jiaqing Wu[1], Jie Gu[1*], Shuqi Liu[1] and Zhijian Jin[1]

Abstract

The construction of integrated energy systems can help improve energy efficiency and promote global energy transition. However, in recent years, the occurrence of extreme natural disasters has brought certain threats to the safe and stable operation of the integrated energy system. Thus, it is necessary to improve the ability of the integrated energy system to resist disasters, reduce disaster losses, and restore energy supply as soon as possible, i.e., improve its resilience. Considering the influence of pre-disaster prevention measures and disaster-time operational measures on system disaster resilience and the correlation between the two, this paper proposes a system hardening strategy based on three-layer robust optimization. The upper layer formulates the optimal hardening strategy of the system before the disaster event occurs, the middle layer identifies the failed elements in the worst disaster situation, while the lower layer realizes the system operational optimization by coordinating the energy storage charging and discharging plan of each subsystem. The strategy can reduce the total supply shortage of the integrated energy system and improve the flexibility of the system in the pre-disaster prevention and disaster resistance integration stages.

Keywords Integrated energy system, Natural disasters, Prevention–resistance, Resilience improvement, Robust optimization

1 Introduction

An Integrated Energy System (IES) is a comprehensive infrastructure system that realizes the coupling of power, heat, refrigeration, natural gas, transportation and other systems. The construction of an IES will help promote global energy transformation, improve comprehensive energy utilization efficiency and the operation of various energy system flexibility [1]. However, in recent years, the occurrence of extreme natural disasters has posed a great threat to the safe and stable operation of IES [2]. In August 2018, an earthquake measuring 6.8 on the Richter scale on Indonesia's Sumbawa Island caused power outages in Lombok Island and northwest Geely islands. In August 2019, an earthquake measuring 6.4 on the Richter scale in the waters off Taiwan caused damage to 2 transmission line towers and the disconnection of a transmission line. More than 700 households suffered power outages and 3 gas pipelines were broken. Therefore, it is necessary to improve the ability of an IES to resist extreme natural disasters, reduce disaster losses and restore energy supply as soon as possible, i.e., to improve its resilience.

At present, research on system resilience improvement technology mainly focuses on the two stages of pre-disaster prevention and post-disaster recovery [3].

*Correspondence:
Jie Gu
gujie@sjtu.edu.cn
[1] Department of Electrical Engineering, School of Electronic Information and Electrical Engineering, Shanghai Jiao Tong University, Shanghai, China

© The Author(s) 2023. **Open Access** This article is licensed under a Creative Commons Attribution 4.0 International License, which permits use, sharing, adaptation, distribution and reproduction in any medium or format, as long as you give appropriate credit to the original author(s) and the source, provide a link to the Creative Commons licence, and indicate if changes were made. The images or other third party material in this article are included in the article's Creative Commons licence, unless indicated otherwise in a credit line to the material. If material is not included in the article's Creative Commons licence and your intended use is not permitted by statutory regulation or exceeds the permitted use, you will need to obtain permission directly from the copyright holder. To view a copy of this licence, visit http://creativecommons.org/licenses/by/4.0/.

The goal of resilience improvement in the pre-disaster prevention stage includes enhancing the system's ability to resist disasters in advance and reducing system losses when disasters penetrate. Among the common resilience improvement measures in the pre-disaster prevention phase, system hardening is the most commonly used and one of the effective strategies to improve system resilience. It can reduce the failure probability and the recovery cost of elements when there are disasters, by improving the black-start capability of the system, configuring distributed power and energy storage, vegetation management, grounding overhead lines, upgrading elements and increasing system redundancy, etc. In terms of element upgrading, reference [4] studies the ability of various measures to improve the resilience of transmission networks under different disaster intensities based on robustness improvement (reinforcing transmission towers and lines), redundancy improvement (installation of double-circuit lines) and rapidity improvement (speeding up fault repair). Reference [5] proposes a risk-oriented weak element identification method to enhance the important towers and towers with high failure probability to improve the resilience of the distribution network. Reference [6] establishes a coordinated optimization model that considers network hardening and distributed power configuration, while [7] studies the impact of different hardening technologies on improving the disaster resistance of distribution networks. However, the above studies are only conducted from the aspect of single energy system enhancement, and do not involve IES considering multi-energy coupling. In terms of multi-energy system hardening, reference [8] analyzes the resilience of the electricity-gas interconnection system during normal and fault operation of the natural gas subsystem in disasters. The results prove that the resilience of the overall system is higher when the two subsystems are coupled in operation. References [9] and [10] construct system hardening models from the perspective of comprehensive planning of power and natural gas subsystems respectively. They use the stronger disaster resistance of gas pipelines to improve grid resilience. However, the mutual influence of pre-disaster prevention measures and disaster-time resilience measures in the process of system resilience is ignored.

This paper combines the optimal planning problem for the pre-disaster prevention stage and the optimal operation problem for the disaster resistance stage to propose a regional integrated energy system (RIES) hardening strategy based on three-layer robust optimization. Its main idea is to develop the optimal pre-disaster line/pipeline hardening plan. In the worst disaster situation, the charging and discharging energy of each energy storage device is adjusted to optimize the operational mode of the RIES in the disaster resistance phase, so as to reduce the total energy supply shortage of the RIES and improve its resilience in the pre-disaster prevention and disaster resistance integration stages.

The main contributions of this paper are as follows:

(1) Based on the definition of RIES resilience, a quantitative method and evaluation index of RIES resilience are proposed, and an analysis framework of RIES resilience is established.
(2) Considering the characteristics of low probability-high loss disaster events and the failure probabilities of different elements of an RIES under different disaster intensities, an RIES resilience improvement model in the pre-disaster prevention and disaster resistance integration stages is proposed based on robust optimization.
(3) A solution strategy based on a column-and-constraint generation algorithm is proposed to analyze the three-layer robust optimization model. This helps reduce the complexity of model calculation by decomposing the defense–attack–defense target model into an outer main problem and an inner subproblem.

The rest of this paper is organized as follows. In Sect. 2, RIES resilience definition, quantification and evaluation are provided. The RIES resilience improvement model framework and its details are described in Sect. 3, while Sect. 4 summarizes the solution process for the optimization model. Results of the proposed optimization model are presented in Sect. 5, where the implementation of the model is discussed. Finally, Sect. 6 concludes the paper and discusses future directions.

2 RIES and its basic concept of resilience

2.1 RIES structure and its resilience definition

In this section, the details of RIES structure and resilience definition are shown.

2.1.1 RIES structure

The research target of this paper is an RIES, which mainly includes power, natural gas, heat and coupling equipment. The coupled equipment includes gas-electricity, gas-heat, electricity-heat and electricity-gas-heat conversion equipment [11]. The structural framework of the RIES is shown in Fig. 1.

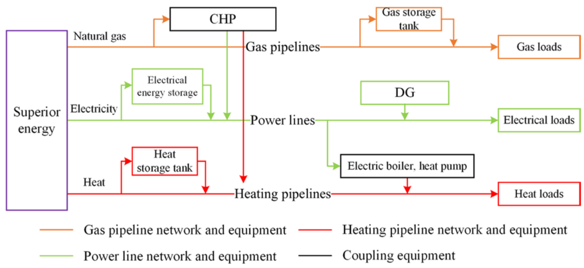

Fig. 1 Framework schematic diagram of regional integrated energy system

2.1.2 RIES resilience definition

Considering the common points of the existing elasticity definitions of various energy systems, this paper defines RIES resilience as the ability of RIES pre-disaster prevention, disaster resistance, disaster response, and post-disaster recovery to the original energy supply state in the face of extreme disaster events with low probability and high loss.

In the pre-disaster prevention stage, the resilience improvement goal mainly includes enhancing the system's ability to resist disasters in advance and reduce system losses when disasters penetrate. In the post-disaster recovery stage, the resilience improvement goal mainly includes improving the system's ability to adapt to the post-disaster state and quickly recover to the original operational level. The pre-disaster prevention stage is crucial to the post-disaster recovery stage and is also the basis of the latter. At the same time, the pre-disaster prevention and disaster resistance are different from the latter two stages. Therefore, in this paper, research mainly focuses on the two stages of pre-disaster prevention and disaster resilience. Resilience research in other stages will be described in another paper.

2.2 RIES resilience quantification and evaluation

2.2.1 Resilience quantification

In view of the low probability and high loss characteristics of extreme disaster events, this paper adopts a deterministic index to quantify RIES resilience. It is defined as the ratio of the actual energy supply level $F_{\mathrm{R}}(t)$ to the expected energy supply level $F_{\mathrm{E}}(t)$ of RIES from the occurrence of the disaster event to the recovery of the system to the normal operating state. The calculation formulas are as follows:

$$R=\frac{\sum\limits_{t\in T}F_{\mathrm{R}}(t)}{\sum\limits_{t\in T}F_{\mathrm{E}}(t)}=1-\frac{\sum\limits_{t\in T}(F_{\mathrm{E}}(t)-F_{\mathrm{R}}(t))}{\sum\limits_{t\in T}F_{\mathrm{E}}(t)}=1-\frac{f_{\mathrm{EL}}}{\sum\limits_{t\in T}F_{\mathrm{E}}(t)} \tag{1}$$

$$\begin{aligned}f_{\mathrm{EL}}&=\sum_{t\in T}(F_{\mathrm{E}}(t)-F_{\mathrm{R}}(t))\\&=\sum_{t\in T}(\sum_{j\in\Omega_N^{\mathrm{e}}}\omega_jL_{j,t}+\sum_{n\in\Omega_N^{\mathrm{g}}}\omega_nL_{n,t}+\sum_{v\in\Omega_N^{\mathrm{h}}}\omega_vL_{v,t})\end{aligned} \tag{2}$$

where R: Resilience of RIES under extreme disaster events. T: The total research period. f_{EL}: The total energy supply shortage of RIES during the research period. Ω_N^{e}, Ω_N^{g}, Ω_N^{h}: Node sets of electricity, natural gas and heat. $L_{j,t}$, $L_{n,t}$, $L_{v,t}$: Energy supply shortages of the power subsystem node j, natural gas subsystem node n and heat subsystem node v at time t. ω_j, ω_n, ω_v: Weight coefficients of electrical load j, gas load n, and heat load v.

2.2.2 Resilience assessment

From (1) and (2), it can be derived that when the expected energy supply level of RIES $F_{\mathrm{E}}(t)$ is a constant, i.e., $F_{\mathrm{E}}(t)=C$, the smaller the total energy supply shortage of the RIES f_{EL}, the greater the resilience R. Thus, the assessment of resilience R can be translated into an assessment of the energy supply shortage of the RIES. Therefore, we will evaluate the impact of disaster events on the RIES and the effectiveness of resilience improvement measures by calculating the energy supply shortage of the RIES.

3 RIES resilience improvement model in the pre-disaster prevention and disaster resistance integration stages

We aim to improve the resilience of the RIES in the pre-disaster prevention and disaster resistant integration stages. Considering the different failure probabilities of different elements of the RIES under disasters [12], a hardening strategy based on three-layer robust optimization is proposed. Some assumptions on which the model is built are shown in the Appendix.

3.1 Objective function

The hardening strategy proposed is a three-layer robust optimization model based on the defense-attack-defense framework. This model minimizes the total energy supply shortage under the worst case by developing the optimal line/pipeline hardening plan before disasters and optimizing system operation during disasters. The logical relationship between each layer is shown in Fig. 2.

The upper-layer model, as the defender, actively determines the optimal network hardening strategy for the upcoming disasters. The middle-layer model, as the attacker, decides the attack situation that can cause the greatest energy supply shortage. The lower-layer model, as the defender, improves the system operational status by optimizing the output of various types of energy storage, in order to minimize the energy supply shortage of the RIES and improve its resilience.

In summary, the objective function can be established as:

$$\min_{\mathbf{h}\in\mathbf{H}} \max_{\mathbf{u}\in\mathbf{U}} \min_{\mathbf{z}\in\mathbf{F}(\mathbf{h},\mathbf{u})} f_{\mathrm{EL}} \tag{3}$$

where **h**: Decision variables of the line/pipeline hardening strategy. **H**: Feasibility set for decision variables. **U**: Uncertain set of failed elements in the RIES caused by natural disasters. **u**: State vector of elements under disaster events. **z**: Decision variables related to the RIES operation. **F**: Feasible RIES operating conditions.

3.2 Constraint condition

3.2.1 Upper-layer model constraints

The constraints of the upper-layer model limit the maximum hardening quantity of lines/pipelines. These are composed of the feasibility set of hardening decisions. The constraints mainly consider the limitations of many factors such as engineering construction capacity and cost, and are defined as:

$$\mathbf{H} = \left\{ \mathbf{h} \middle| \sum_{(i,j)\in\Omega_L^{\mathrm{e}}} \kappa_{ij} h_{ij} + \sum_{(m,n)\in\Omega_L^{\mathrm{g}}} \kappa_{mn} h_{mn} + \sum_{(u,v)\in\Omega_L^{\mathrm{h}}} \kappa_{uv} h_{uv} \le \Delta_h,\ h_{ij}, h_{mn}, h_{uv} \in \{0,1\} \right\} \tag{4}$$

where h_{ij}, h_{mn}, h_{uv}: Binary variables that reflect the hardening state of lines/pipelines. κ_{ij}, κ_{mn}, κ_{uv}: Cost factors required to harden elements of different lengths and types (i.e., lines or pipelines). Δ_h: Hardening level, which can be determined in the following two ways:

(1) In [7], hardening level is calculated based on the material cost required for actual hardening. When the material cost required to harden a certain line or pipeline is known, Δ_h represents the total material cost of the hardening strategy.
(2) Hardening level is calculated based on the labor cost required for the actual hardening. When the manpower required to harden a line or pipeline is known, Δ_h represents the total labor cost of the hardening strategy.

3.2.2 Middle-layer model constraints

The middle-layer model is used to identify the fault events that can cause the maximum resilience loss of the RIES in a specific disaster intensity, and maximize the impact of disaster events. Its constraints consist of an uncertain set of faulty elements caused by disaster events, and are defined as:

$$\mathbf{U} = \left\{ \mathbf{u} \middle| \sum_{(i,j)\in\Omega_L^{\mathrm{e}}} (-\log_2 p_{ij,l}) \cdot u_{ij} + \sum_{(m,n)\in\Omega_L^{\mathrm{g}}} (-\log_2 p_{mn,l}) \cdot u_{mn} + \sum_{(u,v)\in\Omega_L^{\mathrm{h}}} (-\log_2 p_{uv,l}) \cdot u_{uv} \le -\log_2 \Delta_l \right. \tag{5}$$

$$a_{ij,t} = 1,\ t < t_1,\ (i,j) \in \Omega_L^{\mathrm{e}} \tag{6}$$

$$a_{mn,t} = 1,\ t < t_1,\ (m,n) \in \Omega_L^{\mathrm{g}} \tag{7}$$

$$a_{uv,t} = 1,\ t < t_1,\ (u,v) \in \Omega_L^{\mathrm{h}} \tag{8}$$

$$a_{ij,t} = 1 - u_{ij} + u_{ij} \cdot h_{ij},\ t \ge t_1,\ (i,j) \in \Omega_L^{\mathrm{e}} \tag{9}$$

$$a_{mn,t} = 1 - u_{mn} + u_{mn} \cdot h_{mn},\ t \ge t_1,\ (m,n) \in \Omega_L^{\mathrm{g}} \tag{10}$$

$$a_{uv,t} = 1 - u_{uv} + u_{uv} \cdot h_{uv},\ t \ge t_1,\ (u,v) \in \Omega_L^{\mathrm{h}} \tag{11}$$

$$\left. \begin{array}{l} u_{ij}, u_{mn}, u_{uv}, a_{ij}, a_{mn}, a_{uv} \in \{0,1\}, \\ (i,j) \in \Omega_L^{\mathrm{e}}, (m,n) \in \Omega_L^{\mathrm{g}}, (u,v) \in \Omega_L^{\mathrm{h}} \end{array} \right\} \tag{12}$$

where $a_{ij,t}$, $a_{mn,t}$, $a_{uv,t}$: Binary variables that reflect the running state of lines/pipelines. t_1: Disaster occurrence time. u_{ij}, u_{mn}, u_{uv}: Binary variables that reflect the working state of lines/pipelines. $-\log_2 p_{ij,l}$, $-\log_2 p_{mn,l}$, $-\log_2 p_{uv,l}$: Respective resilience coefficients of a single power line, natural gas pipeline and heating pipeline, when the disaster intensity is l.

From the definition of the resilience coefficient, it can be obtained by calculating the failure probability p of the element in disasters. The resilience coefficient reflects the disaster resistance ability of the element, and the higher the value is, the better the element can resist the impact of disasters. It is worth noting that the “failure

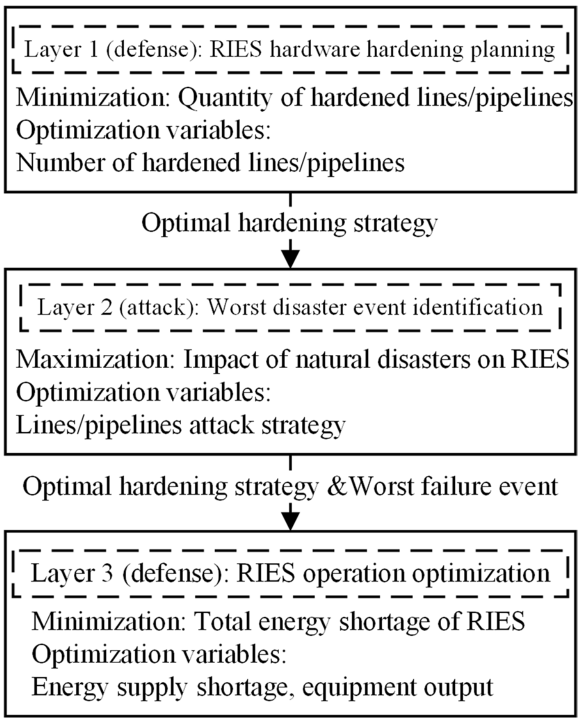

Fig. 2 The internal logical relations of the three-layer robust optimization model

probability" proposed here refers to the short-term failure rate of elements in natural disasters. From a single stage, the failure probability can be assumed to be constant [13, 14] because the four stages can be regarded as Markov chains. The failure probability of elements in each stage remains unchanged, but the failure probability of elements in the next stage is affected by the previous stage. We calculate the failure probability of power lines using the methods in [7] and [15], whereas the failure probability of natural gas pipelines and heating pipelines is calculated by the methods in [2].

In the constraints of the middle-layer model, Eq. (5) describes the impact of disaster events on the system. $-\log_2 \Delta_l$ represents the element failure constraint of RISE when the disaster intensity is l. The value of the parameter Δ_l can be determined by calculating the maximum expected failure order of lines/pipelines and its corresponding maximum expected average failure probability. The specific steps are shown in Fig. 8 in the Appendix.

It should be noted that the initial defined values of K_L^{e}, K_L^{g} and K_L^{h} are only used to calculate Δ_l, and the worst-case fault condition of the line/pipeline is determined by the importance of Δ_l and each line/pipeline to the RIES. From (5), the method proposed in this paper is an extension of the traditional N–K criterion. If the failure probabilities of lines and pipelines are the same, Eq. (5) will be equivalent to the N–K criterion, i.e., at most K lines and pipelines fail in the disaster.

In addition, Eqs. (6–8) indicate that power lines, and gas and heating pipelines are available before the disaster occurs. Equations (9–11) describe the logical relationship between the availability a of a single line/pipeline and the damage u caused by natural disasters after a disaster occurs, and ensure that the hardened lines/pipelines will not fail, while (12) describes the binary constraints of a and u.

3.2.3 Lower-layer model constraints

The constraints of the lower-layer model are the state (i.e., normal or faulty) of each element in disasters and RIES operational constraints of the possible energy supply shortage of each node. They are composed of the operational constraints of each subsystem of the RIES, various types of energy storage devices and each coupling device.

(1) Power subsystem operation constraints

$$P_{ij,t} + P_{j,t}^{\mathrm{chp}} + P_{j,t}^{\mathrm{grid}} + L_{j,t} = \sum_{k \in \pi(j)} P_{jk,t} + P_{j,t}^{\mathrm{ld}} + P_{j,t}^{\mathrm{eb}} \tag{13}$$

$$Q_{ij,t} + Q_{j,t}^{\mathrm{chp}} + Q_{j,t}^{\mathrm{grid}} + L_{j,t} \tan \varphi_{j,t}^{\mathrm{ld}} = \sum_{k \in \pi(j)} Q_{jk,t} + Q_{j,t}^{\mathrm{ld}} \tag{14}$$

$$a_{ij,t}\underline{P}_{ij} \le P_{ij,t} \le a_{ij,t}\overline{P}_{ij} \tag{15}$$

$$a_{ij,t}\underline{Q}_{ij} \le Q_{ij,t} \le a_{ij,t}\overline{Q}_{ij} \tag{16}$$

$$-(1-a_{ij,t})M \le U_{i,t} - U_{j,t} - (R_{ij}P_{ij,t} + X_{ij}Q_{ij,t})/U_0 \le (1-a_{ij,t})M \tag{17}$$

$$\underline{U}_i \le U_i \le \overline{U}_i \tag{18}$$

$$\underline{P}_j^{\mathrm{grid}} \le P_j^{\mathrm{grid}} \le \overline{P}_j^{\mathrm{grid}},\ \underline{Q}_j^{\mathrm{grid}} \le Q_j^{\mathrm{grid}} \le \overline{Q}_j^{\mathrm{grid}} \tag{19}$$

$$\underline{P}_j^{\mathrm{chp}} \le P_{j,t}^{\mathrm{chp}} \le \overline{P}_j^{\mathrm{chp}},\ \underline{Q}_j^{\mathrm{chp}} \le Q_{j,t}^{\mathrm{chp}} \le \overline{Q}_j^{\mathrm{chp}} \tag{20}$$

$$0 \le L_{j,t} \le P_{j,t}^{\mathrm{ld}} \tag{21}$$

where $\varphi_{j,t}^{\mathrm{ld}}$: Power factor angle of load j at time t. $\pi(j)$: Set of distribution network nodes with node j as the parent node. $P_{ij,t}$: Active power flow of the line at time t. $Q_{ij,t}$: Reactive power flow of the line at time t. R_{ij}: Conductance of the line at time t. X_{ij}: Susceptance of the line at time t. M: An arbitrarily large real number. $L_{j,t}$: Energy supply shortage of the power subsystem node j at time t.

(2) Natural gas subsystem operation constraints

$$G_{mn,t} + \beta_{\mathrm{e2g}} P_{n,t}^{\mathrm{gse}} + G_{n,t}^{\mathrm{gs}} + \beta_{\mathrm{e2g}} L_{n,t} = \sum_{o \in \pi(n)} G_{no,t} + G_{n,t}^{\mathrm{ld}} + G_{n,t}^{\mathrm{chp}} + \sum_{(m,n) \in \Omega_C} \eta_{mn} \cdot G_{mn,t} \tag{22}$$

$$-(1 - a_{mn,t})M \le G_{mn,t} - K_{mn} \cdot \sqrt{p_{m,t}^2 - p_{n,t}^2} \le (1 - a_{mn,t})M \tag{23}$$

$$a_{mn,t}\underline{G}_{mn} \le G_{mn,t} \le a_{mn,t}\overline{G}_{mn} \tag{24}$$

$$p_{n,t} \le \omega_{mn} p_{m,t} \tag{25}$$

$$\underline{p}_n \le p_{n,t} \le \overline{p}_n \tag{26}$$

$$0 \le G_{n,t}^{\mathrm{gs}} \le \overline{G}_n^{\mathrm{gs}} \tag{27}$$

$$0 \le L_{n,t} \le G_{n,t}^{\mathrm{ld}} \tag{28}$$

where $G_{mn,t}$: Natural gas flow through the pipeline (m, n) at time t. $P_{n,t}^{\mathrm{gse}}$: Natural gas flow of gas energy storage injection node n. $G_{n,t}^{\mathrm{gs}}$: Natural gas flow of gas source injection node n. $\pi(n)$: Set of gas distribution network nodes with node n as the parent node. $G_{n,t}^{\mathrm{ld}}$: Gas load at node n at time t. $G_{n,t}^{\mathrm{chp}}$: Demand for electricity-gas-heat coupling equipment at node n at time t. Ω_C: Set of pipelines connected to the compressor. β_{e2g}: Electricity to gas coefficient. η_{mn}: Compression efficiency. ω_{mn}: Compression ratio. $p_{n,t}$: Air pressure at node n at time t. K_{mn}: Calculation parameter of the pipeline (m, n).

(3) Heat subsystem operational constraints

$$\sum_{b \in F(u)} m_{b,t}^{\mathrm{s}} + m_{u,t}^{\mathrm{ld}} + \beta_{\mathrm{e2h}} L_{u,t} = m_{u,t}^{\mathrm{g}} + m_{u,t}^{\mathrm{hse}} + \sum_{b \in T(u)} m_{b,t}^{\mathrm{s}} \tag{29}$$

$$\sum_{b \in F(u)} m_{b,t}^{\mathrm{r}} + m_{u,t}^{\mathrm{g}} + m_{u,t}^{\mathrm{hse}} = m_{u,t}^{\mathrm{ld}} + \beta_{\mathrm{e2h}} L_{u,t} + \sum_{b \in T(u)} m_{b,t}^{\mathrm{r}} \tag{30}$$

$$\sum_{b \in F(u)} (\tau_{b,t}^{\mathrm{s,out}} m_{b,t}^{\mathrm{s}}) = \tau_{u,t}^{\mathrm{s}} \sum_{b \in T(u)} m_{b,t}^{\mathrm{s}} \tag{31}$$

$$\sum_{b \in F(u)} (\tau_{b,t}^{\mathrm{r,out}} m_{b,t}^{\mathrm{r}}) = \tau_{u,t}^{\mathrm{r}} \sum_{b \in T(u)} m_{b,t}^{\mathrm{r}} \tag{32}$$

$$\begin{cases} \tau_{b,t}^{\mathrm{s,in}} = \tau_{u,t}^{\mathrm{s}} \\ \tau_{b,t}^{\mathrm{r,in}} = \tau_{u,t}^{\mathrm{r}} \end{cases} \tag{33}$$

$$0 \le m_{b,t}^{\mathrm{s}}, m_{b,t}^{\mathrm{r}} \le m_b^{\mathrm{max}} \tag{34}$$

$$pr_{u,t}^{\mathrm{s}} - pr_{v,t}^{\mathrm{s}} = \mu_b (m_{b,t}^{\mathrm{s}})^2 \tag{35}$$

$$pr_{v,t}^{\mathrm{r}} - pr_{u,t}^{\mathrm{r}} = \mu_b (m_{b,t}^{\mathrm{r}})^2 \tag{36}$$

$$\tau_{b,t}^{\mathrm{s,out}} = (\tau_{b,t}^{\mathrm{s,in}} - \tau_t^{\mathrm{am}}) e^{-\frac{\lambda_b L_b}{c_{\mathrm{w}} m_{b,t}^{\mathrm{s}}}} + \tau_t^{\mathrm{am}} \tag{37}$$

$$\tau_{b,t}^{\mathrm{r,out}} = (\tau_{b,t}^{\mathrm{r,in}} - \tau_t^{\mathrm{am}}) e^{-\frac{\lambda_b L_b}{c_{\mathrm{w}} m_{b,t}^{\mathrm{r}}}} + \tau_t^{\mathrm{am}} \tag{38}$$

$$d_{u,t}^{\mathrm{wp}} = m_{u,t}^{\mathrm{g}} \frac{pr_{u,t}^{\mathrm{s}} - pr_{u,t}^{\mathrm{r}}}{\eta_u^{\mathrm{wp}} \rho} \tag{39}$$

$$d_u^{\mathrm{wp,min}} \le d_{u,t}^{\mathrm{wp}} \le d_u^{\mathrm{wp,max}} \tag{40}$$

where $F(u)$: Pipeline set with node u as the parent node. $T(u)$: Pipeline set with node u as the child node. $m_{b,t}^{\mathrm{s}}$, $m_{b,t}^{\mathrm{r}}$: Mass flow rates of circulating water in the supply/return water system pipeline b at time t. $m_{u,t}^{\mathrm{g}}$, $m_{u,t}^{\mathrm{hse}}$, $m_{u,t}^{\mathrm{ld}}$: Circulating water mass flow rates of the heat source equipment, heat energy storage and heat load at node u. β_{e2h}: electricity to heat coefficient. $\tau_{u,t}^{\mathrm{s}}$, $\tau_{u,t}^{\mathrm{r}}$: Temperatures of the node u of the supply/return water system. $pr_{u,t}^{\mathrm{s}}$, $pr_{v,t}^{\mathrm{r}}$: Inlet pressures of the pipeline b in the supply/return water system at time t. $pr_{v,t}^{\mathrm{s}}$, $pr_{u,t}^{\mathrm{r}}$: Outlet pressures of the pipeline b in the supply/return water system at time t. μ_b: Pressure loss coefficient of the pipeline b. λ_b: Temperature loss coefficient of the pipeline b. L_b: Length of the pipeline b. τ_t^{am}: Ambient temperature at time t. $d_{u,t}^{\mathrm{wp}}$: Electrical energy consumed by the circulating water pump configured at node u at time t. ρ: Density of circulating water. η_u^{wp}: Efficiency of the circulating water pump.

Equation sets (29–38) and (39–40) describe the operational constraints of heating pipelines and the circulating water pump, respectively.

(4) Coupling equipment operational constraints

The energy coupling characteristics of RIES are mainly realized by coupling devices between various subsystems. They mainly include gas-electricity, gas-heat and electricity-heat coupling devices that realize two types of energy coupling, and electricity-gas-heat coupling devices that realize three types of energy coupling.

(i) Gas-electricity coupling equipment: gas turbine (GT)

$$P_{i,t}^{g2e} = \frac{V_{i,t}^{g2e} \underline{L}^{g} \eta^{g2e}}{\Delta t} \tag{41}$$

where $V_{i,t}^{\mathrm{g2e}}$: Input natural gas power of GT at node i at time t. $P_{i,t}^{\mathrm{g2e}}$: Output electrical power of GT at node i at time t. $\underline{L}^{\mathrm{g}}$: Low calorific value of natural gas. η^{g2e}: Power generation efficiency of GT.

(ii) Gas-heat coupling equipment: gas boiler (GB)

$$h_{i,t}^{\mathrm{g2h}} = \frac{V_{i,t}^{\mathrm{g2h}} \underline{L}^{\mathrm{g}} \eta^{\mathrm{g2h}}}{\Delta t} \tag{42}$$

where $V_{i,t}^{\mathrm{g2h}}$: Input natural gas power of GB at node i at time t. $h_{i,t}^{\mathrm{g2h}}$: Output heat power of GB at node i at time t. η^{g2h}: Heat generation efficiency of GB.

(iii) Electricity-heat coupling equipment: electric boiler (EB)

$$h_{i,t}^{\mathrm{chp}} + h_{i,t}^{\mathrm{eb}} = c_{\mathrm{w}} m_{i,t}^{\mathrm{g}} (\tau_{i,t}^{\mathrm{s}} + \tau_{i,t}^{\mathrm{r}}) \tag{43}$$

$$\tau_i^{\mathrm{s,min}} \le \tau_i^{\mathrm{s}} \le \tau_i^{\mathrm{s,max}} \tag{44}$$

$$d_i^{\mathrm{eb,min}} \le d_i^{\mathrm{eb}} \le d_i^{\mathrm{eb,max}} \tag{45}$$

where $h_{i,t}^{\mathrm{chp}}$: Heat energy supplied by CHP at node i at time t. c_{w}: Specific heat capacity at constant pressure of the circulating water. $\tau_i^{\mathrm{s,max}}$, $\tau_i^{\mathrm{s,min}}$: Upper and lower temperature limits of the water supply at node i. $d_i^{\mathrm{eb,max}}$, $d_i^{\mathrm{eb,min}}$: Upper and lower limits of the power consumption of EB at node i.

(iv) Electricity-gas-heat coupling equipment: Combined Heat and Power (CHP).

In this paper, the electricity/gas/heat coupling link is realized by CHP, and the energy coupling relationship can be described by the energy hub, whose basic structure is shown in Fig. 3 [16].

The CHP used in this paper is composed of a power transformer, micro GT and GB. The input energy are electricity and natural gas (P_{e} and P_{g}), respectively. The former is directly input to the transformer, while the latter is input to GT and GB at the same time. The output energy is electrical and heat energy, L_{e} and L_{h}, respectively. The former is supplied by the transformer and GT, while the latter is jointly supplied by GB and GT. The input/output energy coupling relationship can be represented as:

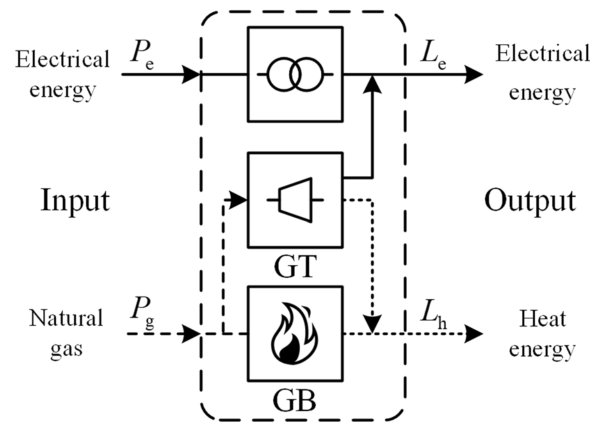

Fig. 3 Energy hub topology

$$\underbrace{\begin{bmatrix} L_{\mathrm{e}} \\ L_{\mathrm{h}} \end{bmatrix}}_{\mathbf{L}} = \underbrace{\begin{bmatrix} \eta^{\mathrm{T}} & \nu^{\mathrm{gt}} \eta_{\mathrm{g2e}}^{\mathrm{gt}} \\ 0 & \nu^{\mathrm{gt}} \eta_{\mathrm{g2h}}^{\mathrm{gt}} + (1-\nu^{\mathrm{gt}}) \eta^{\mathrm{gb}} \end{bmatrix}}_{\mathbf{C}} \underbrace{\begin{bmatrix} P_{\mathrm{e}} \\ P_{\mathrm{g}} \end{bmatrix}}_{\mathbf{P}} \tag{46}$$

where $\eta_{\mathrm{g2e}}^{\mathrm{gt}}$: Gas-to-electricity efficiency of GT. $\eta_{\mathrm{g2h}}^{\mathrm{gt}}$: Gas-to-heat efficiency of GT. η^{T}: Transformer efficiency. $\boldsymbol{P}$: Input energy matrix. $\boldsymbol{L}$: Output energy matrix. $\boldsymbol{C}$: Coupling matrix.

In addition, the coupling coefficient is related not only to the conversion efficiency of the coupling device, but also to the distribution ratio of energy in different coupling devices. Therefore, the distribution coefficients ν^{gt} $(0 \le \nu^{\mathrm{gt}} \le 1)$, $(1-\nu^{\mathrm{gt}})P_{\mathrm{g}}$ and $\nu^{\mathrm{gt}} P_{\mathrm{g}}$ are introduced to represent the natural gas power input into GB and GT, respectively.

In summary, Eqs. (41–46) constitute the coupling device constraints of the RIES studied here.

(5) Energy storage equipment operational constraints

The operating characteristics of electric, heat and gas energy storages in the RIES are basically the same [17]. In order to better reflect the coordination relationship among the three, the state of energy (SOE) constraints are defined as:

$$S_{i,t}=S_{i,0}(1-\sigma_i)^t+\sum_{\tau=1}^{t}\left(\frac{P_{i,\tau}^{\mathrm{s}}}{E_{i,\mathrm{n}}}\eta_i^{\mathrm{s}}-\frac{P_{i,\tau}^{\mathrm{r}}}{\eta_i^{\mathrm{r}}E_{i,\mathrm{n}}}\right)\Delta t \quad (47)$$

$$\begin{cases} S_{i,\min}\le S_{i,t}\le S_{i,\max} \\ 0\le P_{i,t}^{\mathrm{r}}\le z_{i,t}^{\mathrm{r}}P_{i,n} \\ 0\le P_{i,t}^{\mathrm{s}}\le z_{i,t}^{\mathrm{s}}P_{i,n} \\ z_{i,t}^{\mathrm{r}}+z_{i,t}^{\mathrm{s}}\le 1 \\ P_{i,t}=P_{i,t}^{\mathrm{r}}-P_{i,t}^{\mathrm{s}} \end{cases} \quad (48)$$

where $S_{i,t}$: Energy state of the energy storage device i. σ_i: Self-discharge coefficient of the energy storage device i. $P_{i,\tau}^{\mathrm{s}}$,$P_{i,\tau}^{\mathrm{r}}$: Charging and discharging power of the energy storage device i at time τ. η_i^{s}, η_i^{r}: Charging and discharging efficiencies of the energy storage device i. $E_{i,\mathrm{n}}$: Rated capacity of the energy storage device i. $z_{i,t}^{\mathrm{s}}$, $z_{i,t}^{\mathrm{r}}$: Binary variables that represent the states of charging and discharging of energy storage device i. $P_{i,t}$: The total charge and discharge power of the energy storage device i at time t.

4 Model solution

The three-layer robust optimization model based on RIES resilience boosting established here conforms to the framework of a column-and-constraint generation (CCG) algorithm. The defense-attack-defense target model is decomposed into an outer main problem and an inner subproblem through this algorithm. The optimal solution with limited convergence is obtained through continuous iterative solutions.

4.1 Model simplification

Because of the non-linearity of the energy supply network and the 0–1 constraints of the energy storage charging and discharging states, the model is a mixed integer nonlinear programming problem. In this paper, the nonlinear terms in the electric/heat and gas subsystems are linearized by the methods proposed in [18] and [19] respectively, to reduce the difficulty of solution.

4.2 Model solution procedure

Before solving the model, Eq. (3) is expressed as the standard form of the CCG algorithm, as:

$$\min_{\mathbf{h}\in\mathbf{H}}\max_{\mathbf{u}\in\mathbf{U}}\min_{\mathbf{z}\in\mathbf{F}(\mathbf{h},\mathbf{u})}\mathbf{c}^{\mathrm{T}}\mathbf{z} \quad (49)$$

where $\mathbf{F}(\mathbf{h},\mathbf{u})=\{\mathbf{z}:\mathbf{Gz}+\mathbf{Eh}+\mathbf{Mu}\ge\mathbf{g}\}$ corresponds to the linearized RIES system constraint and is a linear function of $\mathbf{u}$. $\mathbf{G}$, $\mathbf{E}$, and $\mathbf{M}$ are constant coefficient matrices, and $\mathbf{c}$ and $\mathbf{g}$ are constant coefficient vectors, all of which are composed of deterministic values. Uncertainty is reflected in the vector $\mathbf{u}$.

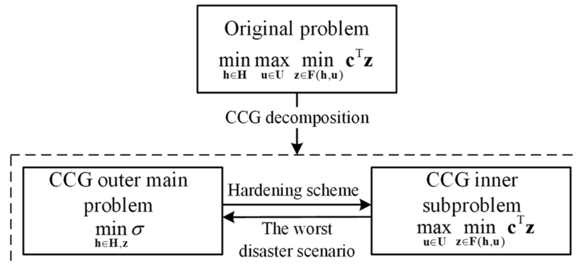

Fig. 4 The decomposition results of CCG algorithm

Then, Eq. (49) is decomposed into an outer main problem and an inner subproblem for iterative solution, as shown in Fig. 4.

4.2.1 The CCG inner subproblem

In Fig. 4, the inner subproblem determines the worst disaster scenario that causes the maximum energy supply shortage of the RIES in the given line/pipeline hardening scheme, which is then returned to the outer main problem. Its model is defined as:

$$y(\hat{\mathbf{h}})=\max_{\mathbf{u}\in\mathbf{U}}\min_{\mathbf{z}\in\mathbf{F}(\mathbf{h},\mathbf{u})}\mathbf{c}^{\mathrm{T}}\mathbf{z} \quad (50)$$

$$\text{s.t.}\mathbf{Gz}+\mathbf{E}\hat{\mathbf{h}}+\mathbf{Mu}\ge\mathbf{g}:(\boldsymbol{\lambda}) \quad (51)$$

where decision variable $\hat{\mathbf{h}}$ is the hardening scheme provided by the outer main problem, and $\boldsymbol{\lambda}$ is the dual variable of the inner linear programming problem.

The inner subproblem is essentially a two-layer optimization problem, and the solution can follow a similar path to the original problem. The upper-layer model generates the worst disaster event under the given line/pipeline hardening scheme according to the RIES energy supply shortage returned by the lower-layer model, whereas the lower-layer model optimizes the line/pipeline hardening scheme according to the fault scenarios provided by the upper-layer model. In addition, the duality theory is applied to the linear programming model in the upper layer of (50). The inner layer subproblem can be equivalently transformed into a single-layer bilinear maximization problem, as:

$$y(\hat{\mathbf{h}})=\max_{\mathbf{u}\in\mathbf{U},\boldsymbol{\lambda}}(\mathbf{g}-\mathbf{E}\hat{\mathbf{h}}-\mathbf{Mu})^{\mathrm{T}}\boldsymbol{\lambda} \quad (52)$$

$$\text{s.t.}\mathbf{G}^{\mathrm{T}}\boldsymbol{\lambda}\le\mathbf{c},\boldsymbol{\lambda}\ge 0 \quad (53)$$

The bilinear term $(\mathbf{Mu})^{\mathrm{T}}\boldsymbol{\lambda}$ in the objective function can be introduced into the auxiliary continuous variable r, which can be linearized with the large M method, and further transformed into a mixed integer linear programming problem, as:

$$r = u \cdot \lambda \tag{54}$$

$$-u \cdot M \le r \le 0 \tag{55}$$

$$\lambda - (1-u) \cdot M \le r \le \lambda + (1-u) \cdot M \tag{56}$$

4.2.2 The CCG outer main problem

In Fig. 1, the outer main problem automatically adds a new set of hardening schemes (i.e., decision variables) of lines/pipelines and a new lower bound of the original problem based on the worst disaster scenario obtained by each iteration of the inner subproblem. Its model is defined as:

$$\min_{\mathbf{h} \in \mathbf{H}, \mathbf{z}} \sigma \tag{57}$$

$$\text{s.t.}\sigma \ge \mathbf{c}^{\mathrm{T}}\mathbf{z}_w;\ \mathbf{G}\mathbf{z}_w + \mathbf{E}\mathbf{h} + \mathbf{M}\hat{\mathbf{u}}_w \ge \mathbf{g}\ \forall w \in \mathbf{W} \tag{58}$$

The variable σ introduced in (57) ensures that the optimal solution of the outer main problem strictly satisfies the constraints for all situations in the uncertain set, while $\mathbf{W}$ represents the worst disaster scenario set obtained iteratively in the inner subproblem. If $\mathbf{W}$ contains all disaster scenarios, the outer main problem is equivalent to the original problem.

The outer main problem replaces the uncertain set of the original problem with the deterministic set of the inner subproblem. The actual solution is a relaxed solution of the original problem. Therefore, the outer main problem does not have the uncertainty of the original problem, i.e., the outer main problem also belongs to a simple MILP problem.

To sum up, the CCG algorithm decomposes the RIES hardening problem for resilience improvement into the subproblem of identifying the worst disaster events and the main problem of generating the best hardening strategy. It is iteratively solved through the inner and outer double loops. The specific algorithm solution process is shown in Fig. 9 in the Appendix.

5 Case study

In order to verify the effectiveness of the three-layer robust optimization model based on RIES resilience improvement, we analyze and verify the RIES test system composed of the modified IEEE 33-bus distribution network, the Belgian 20-bus gas distribution network and the Balinese 32-bus heat distribution network. The system topology is shown in Fig. 10 in the Appendix [20].

5.1 Case parameters

The main parameters of the RIES test system used in this paper are:

(1) The distribution network consists of 33 nodes, 32 distribution lines, 32 electrical loads and 1 electrical energy storage.
(2) The gas distribution network consists of 20 nodes, 2 natural gas sources, 17 gas distribution pipelines, 2 compressors, 15 gas loads and 1 gas energy storage.
(3) The heat distribution network contains a total of 32 nodes, 32 heating pipelines, 18 heat loads and 1 heat storage unit.
(4) The parameters of each energy storage are shown in Table 8 in the Appendix.
(5) The energy coupling equipment includes 2 CHP units and 1 EB, and their capacity parameters are shown in Table 9 in the Appendix.
(6) The typical daily load value of each subsystem of the RIES is shown in Fig. 11 in the Appendix. As in [19], this paper divides the load into 5 levels, as shown in Table 10 in the Appendix.
(7) The hardening coefficients of power lines, heating pipelines, and gas pipelines are set to 1, 2, and 3 respectively, to indicate that hardening buried pipelines requires more labor and material costs than overhead lines.

5.2 Scheme set-up

In order to verify the superiority of the proposed model, the following schemes are set for comparative analysis:

(1) *Scheme 1* RIES robust optimization model for line N–K fault in natural disasters
(2) *Scheme 2* RIES robust optimization model of line/pipeline failure probability in natural disasters

The objective function of the robust optimization model described in scheme 1 is still (3), but the uncertain set of failure of lines/pipelines in disasters is defined as:

Table 1 System parameters with respect to different disaster intensities

Disaster intensity	Maximum expected fault order of lines/pipelines	$(p_{ij,l}, p_{mn,l}, p_{uv,l})$	Δl
1	(2,0,1)	(0.2,0.03,0.05)	2×10^{-3}
2	(2,1,1)	(0.3,0.05,0.08)	3.6×10^{-4}
3	(2,2,2)	(0.4,0.1,0.17)	4.6×10^{-5}
4	(3,3,3)	(0.6,0.13,0.24)	6.6×10^{-6}
5	(4,4,3)	(0.7,0.2,0.33)	1.4×10^{-5}

$$\mathbf{U} = \left\{ \mathbf{u} \left| \sum_{(i,j)\in\Omega_L^{\mathrm{e}}} a_{ij,t} \geq N_L^{\mathrm{e}} - K_L^{\mathrm{e}}, \sum_{(m,n)\in\Omega_L^{\mathrm{g}}} a_{mn,t} \geq N_L^{\mathrm{g}} - K_L^{\mathrm{g}}, \sum_{(u,v)\in\Omega_L^{\mathrm{g}}} a_{uv,t} \geq N_L^{\mathrm{h}} - K_L^{\mathrm{h}} \right. \right\} \tag{59}$$

where N_L^{e}, N_L^{g} and N_L^{h} represent the total numbers of lines or pipelines in the distribution, gas distribution, and heat distribution networks, respectively.

The operational constraints contained in this model are consistent with the model proposed in this paper, and the CCG algorithm framework is also used to solve it.

5.3 Results and discussion

5.3.1 Analysis of worst disaster events in the RIES

The failure probabilities of power lines, gas and heating pipelines under different disaster intensities are calculated according to the method proposed in Sect. 3.2.2, and the total resilience coefficient of the RIES Δl is then obtained. The results are shown in Table 1.

Subsequently, without system hardening, the worst disaster events of the RIES under different disaster intensities are identified, and the corresponding maximum energy supply shortage of the RIES is calculated. The results are shown in Table 2.

In Table 2, L_{i-j}^{e}, L_{m-n}^{g} and L_{u-v}^{h} represent the power lines, gas and heating pipelines that fail in the disaster, respectively. Combining Tables 1 and 2, the following conclusions can be drawn:

(1) With the increase of disaster intensity, the failure probability of lines and pipelines gradually increases, and the total energy supply shortage of the RIES is also greater.
(2) The system with buried pipelines has higher resilience than that with overhead lines, and is less likely to be damaged in natural disasters with lower strength. In addition, since natural gas is one of the main energy inputs of CHP, damaged gas pipelines will lead to a high energy supply shortage in severe natural disasters.
(3) When the disaster intensity is level 1, i.e. not enough to damage natural gas pipelines, the worst fault condition obtained in Scheme 2 is the fault of two power lines and one heating pipeline, while the result obtained in Scheme 1 is the fault of two gas distribution pipelines and one power line. Similarly, for the disaster intensity of levels 2–4, the total energy shortage of the RIES obtained in Scheme 1 is higher, and more gas distribution pipelines are damaged. It can be seen that the results obtained by using the *N*–*K* criterion reflect the importance of gas distribution pipelines in the RIES, but cannot accurately describe the real impact of natural disasters on overhead lines and buried pipelines. Thus, it does not consider that the resilience of the system with gas distribution pipelines is much higher than that of the system with distribution lines. This is not conducive to helping decision makers formulate the most effective network hardening strategies.

Table 2 Worst-case damages at different intensities

Disaster intensity	Scheme 2			Scheme 1	
	Failed elements	Number of faults	Supply shortage(kW)	Number of faults	Supply shortage(kW)
1	$L_{1-2}^{\mathrm{e}}, L_{6-7}^{\mathrm{e}}, L_{28-31}^{\mathrm{h}}$	(2,0,1)	267.61	(1,2,0)	1931.80
2	$L_{1-2}^{\mathrm{e}}, L_{28-29}^{\mathrm{e}}, L_{8-9}^{\mathrm{g}} L_{28-31}^{\mathrm{h}}$	(2,1,1)	2102.48	(1,2,1)	2548.10
3	$L_{1-2}^{\mathrm{e}}, L_{28-29}^{\mathrm{e}}, L_{1-2}^{\mathrm{g}} L_{8-9}^{\mathrm{g}}, L_{11-13}^{\mathrm{h}}, L_{28-31}^{\mathrm{h}}$	(2,2,2)	2816.43	(1,3,2)	3091.83
4	$L_{1-2}^{\mathrm{e}}, L_{6-26}^{\mathrm{e}}, L_{28-29}^{\mathrm{e}}, L_{1-2}^{\mathrm{g}}, L_{5-6}^{\mathrm{g}} L_{8-9}^{\mathrm{g}}, L_{11-13}^{\mathrm{h}}, L_{14-15}^{\mathrm{h}}, L_{28-31}^{\mathrm{h}}$	(3,3,3)	3243.29	(2,5,2)	3438.43
5	$L_{1-2}^{\mathrm{e}}, L_{6-26}^{\mathrm{e}}, L_{10-11}^{\mathrm{e}}, L_{28-29}^{\mathrm{e}}, L_{1-2}^{\mathrm{g}}, L_{8-9}^{\mathrm{g}}, L_{11-12}^{\mathrm{g}}, L_{11-17}^{\mathrm{g}}, L_{11-13}^{\mathrm{h}}, L_{14-15}^{\mathrm{h}}, L_{28-31}^{\mathrm{h}}$	(4,4,3)	3782.78	(4,4,3)	3782.78

Table 3 Hardening strategies corresponding to different hardening budgets of scheme 1

Hardening budget	Hardened lines/pipelines	Total supply shortage(kW)
1	P^{g}_{8-9}	1757.86
2	P^{g}_{1-2}, P^{g}_{8-9}	1686.18
3	$L^{e}_{1-2}, P^{g}_{8-9}, L^{h}_{14-15}$	1616.36
4	$L^{e}_{1-2}, P^{g}_{1-2}, P^{g}_{8-9}, L^{h}_{14-15}$	1576.83
5	$L^{e}_{1-2}, P^{e}_{6-7}, P^{g}_{1-2}, P^{g}_{8-9}, L^{h}_{2-4}$	1523.62
6	$L^{e}_{1-2}, L^{e}_{6-26}, P^{g}_{1-2}, P^{g}_{8-9}, L^{h}_{2-4}, L^{h}_{14-15}$	1456.83
7	$L^{e}_{1-2}, L^{e}_{27-28}, P^{g}_{5-6}P^{g}_{8-9}, P^{g}_{11-17}, L^{h}_{2-4}, L^{h}_{14-15}$	1416.13
8	$L^{e}_{1-2}, P^{e}_{6-7}, L^{e}_{27-28}, P^{g}_{5-6}, P^{g}_{8-9}, P^{g}_{11-17}, L^{h}_{2-4}, L^{h}_{14-15}$	1348.27
9	$L^{e}_{1-2}, L^{e}_{6-26}, L^{e}_{27-28}, P^{g}_{1-2}, P^{g}_{5-6}, P^{g}_{8-9}, L^{h}_{2-4}L^{h}_{5-6}, L^{h}_{14-15}$	1303.68
10	$L^{e}_{1-2}, P^{e}_{6-7}, L^{e}_{6-26}, P^{g}_{1-2}, P^{g}_{8-9}, P^{g}_{9-10}, P^{g}_{11-17}, L^{h}_{2-4}, L^{h}_{5-6}, L^{h}_{14-15}$	1289.23

Table 4 Hardening strategies corresponding to different hardening budgets of Scheme 2

Hardening budget	Hardened lines/pipelines	Total supply shortage (kW)
1	P^{e}_{1-2}	1553.18
2	P^{e}_{1-2}, P^{g}_{8-9}	1478.42
3	$P^{e}_{1-2}, P^{g}_{8-9}, L^{h}_{14-15}$	1432.81
4	$P^{e}_{1-2}, P^{e}_{6-7}, P^{g}_{8-9}, L^{h}_{14-15}$	1393.82
5	$L^{e}_{1-2}, P^{e}_{6-7}, P^{g}_{8-9}, P^{g}_{10-11}, L^{h}_{14-15}$	1331.83
6	$L^{e}_{1-2}, P^{e}_{6-7}, L^{e}_{27-28}, P^{g}_{8-9}, L^{h}_{11-13}, L^{h}_{14-15}$	1293.62
7	$L^{e}_{1-2}, P^{e}_{6-7}, L^{e}_{27-28}, P^{g}_{8-9}, P^{g}_{10-11}, L^{h}_{11-13}, L^{h}_{14-15}$	1253.86
8	$L^{e}_{1-2}, P^{e}_{6-7}, L^{e}_{27-28}, P^{g}_{8-9}, P^{g}_{9-10}, P^{g}_{10-11}, L^{h}_{11-13}, L^{h}_{14-15}$	1226.21
9	$L^{e}_{1-2}, P^{e}_{6-7}, L^{e}_{27-28}, P^{g}_{8-9}, P^{g}_{9-10}, P^{g}_{10-11}, L^{h}_{5-6}, L^{h}_{11-13}, L^{h}_{14-15}$	1185.00
10	$L^{e}_{1-2}, P^{e}_{6-7}, L^{e}_{6-26}, L^{e}_{27-28}, P^{g}_{8-9}, P^{g}_{9-10}, P^{g}_{10-11}, L^{h}_{5-6}, L^{h}_{11-13}, L^{h}_{14-15}$	1128.03

To sum up, the traditional *N*–*K* criterion is beneficial for determining the importance of elements in the RIES, but it cannot reflect the actual disaster situation of the RIES at different disaster intensities. In contrast, the method proposed in this paper can accurately simulate the real worst failure situation of each element of the RIES in natural disasters of different intensities. It does this by calculating the failure probability of different elements in disasters and assigning different resilience coefficients to overhead lines and buried pipelines.

5.3.2 Analysis of RIES hardening strategy

Based on the results in the previous section, the disaster intensity is set at level 3, and the expected damage order of the lines/pipelines of each subsystem of the RIES is [2, 2, 2]. The comparison results of the line/pipeline hardening strategies and the corresponding total energy supply shortage under the two schemes are shown in Tables 3 and 4, respectively.

Comparing and analyzing the hardening strategies in Tables 3 and 4, the following conclusions can be drawn:

(1) With the increase in hardening budgets of lines/pipelines, the total energy supply shortages of the RIES under the two schemes become smaller and smaller. However, for the same hardening budgets, the total energy supply shortage under Scheme 2 is lower than that under Scheme 1.
(2) When the hardening budget is less than 5, the optimal hardening strategy under Scheme 2 is more inclined to harden the power lines. This is because the proposed model considers that buried pipelines have lower failure probability than overhead lines in disasters. Scheme 1 does not consider the failure probability of lines and pipelines in disasters, and only determines the hardening strategy by identifying the fault conditions that can cause the

maximum energy supply shortage. Therefore, the optimal hardening strategy under Scheme 1 is more inclined to harden gas pipelines.

(3) The hardening scheme of Scheme 2 presents an orderly change with the increase of hardening budgets. The strategy with more hardening budgets is bound to include the strategy with fewer hardening budgets. However, the hardening strategies of Scheme 1 under different hardening budgets are less relevant. This is not conducive to helping decision makers determine the priority of hardened lines/pipelines.

(4) When the hardening budget is large enough (greater than 6), more power lines and heating pipelines are gradually included in the hardening strategies under both schemes. This further reduces the total energy supply shortage of the RIES. When the hardening budget reaches 10, 4 power lines, 3 gas pipelines and 3 heating pipelines in Scheme 2 are hardened. The total energy shortage of the RIES is reduced by 27% compared to when the hardening budget is 1.

(5) By comparing and analyzing the hardening strategies under different hardening budget settings, the proposed system hardening strategy can also reflect the importance of a certain line or pipeline in maintaining the resilience level of the RIES. For example, power line L^{e}_{1-2} and gas pipeline P^{g}_{8-9} are directly connected to the upper-level power supply and gas source, respectively, and once they fail, it will bring a large power supply shortage to the RIES. Therefore, they are of the highest importance and will be prioritized for hardening.

5.3.3 Analysis of influence of energy storage equipment on RIES resilience improvement

When an RIES is attacked by natural disasters, if the power supply of the power grid is interrupted, the electrical energy storage can guarantee the power supply of key electrical loads. Equally, when the main natural gas supply from natural gas retailers is interrupted or curtailed, gas storage tanks in the gas distribution network can also guarantee the supply of gas to key gas loads. Similarly, in the event of failure of the lines/pipelines delivering electrical/gas energy to CHP or electricity to EB, the heat storage tank can provide heat supply for key heat loads. In this paper, by comparing the energy supply shortages of the RIES at different disaster intensities, the importance of energy storage equipment in improving the resilience of the RIES is studied.

In order to verify the effectiveness of the three-layer robust optimization model based on RIES resilience improvement for coordinated energy storage output, four different schemes are added on the basis of Scheme 2, as shown in Table 5.

Table 5 Configuration of schemes 2–6

Scheme	Electrical energy storage	Gas energy storage	Heat energy storage
Scheme 2	√	√	√
Scheme 3	×	√	√
Scheme 4	√	×	√
Scheme 5	√	√	×
Scheme 6	×	×	×

The hardening budget for fixed lines/pipelines is 3, and the hardening results can be found in Table 3. Using the proposed model, the energy supply shortages of the RIES and its subsystems with five energy storage configuration schemes are calculated, as shown in Table 6.

The following conclusions can be drawn from the analysis of Table 6:

(1) For the five schemes listed above, the total energy supply shortage of RIES increases with the increase of disaster intensity. In addition, for each disaster intensity, without the support of heat energy storage, the heat load connected to the end of the failed heating pipeline would be completely removed, resulting in higher heating shortages in Schemes 3 and 4 than that in Scheme 2. Similarly, compared with other schemes, the total gas supply shortages in Schemes 4 and 6 are also significantly increased.

(2) In Scheme 6, if there is no energy storage equipment participating in the operation optimization, the RIES will face the highest energy supply shortage. Therefore, the optimal operation of energy storage equipment can effectively improve the ability of the RIES to resist disaster risks, enhance its flexibility, reduce energy supply shortage in disasters, and provide an important guarantee for the safe and economic operation of the system.

(3) Without gas storage support, the gas supply shortages in Schemes 4 and 6 are significantly higher than those in the other schemes. The reason is that under these two schemes, electrical energy storage is used to give priority to supplying important loads when the power supply of the upper power grid is interrupted, while the lack of gas energy storage will further aggravate the shortage of natural gas supply. Therefore, the lower priority gas loads at the gas distribution network node 12 will be cut off, while

Table 6 Energy losses of RIES and its subsystems at different disaster intensities

Disaster intensity	1	2	3	4	5	
Scheme 2	Electricity (kW)	71.07	204.41	204.41	204.41	356.41
	Gas (kW)	0.00	817.44	1101.91	1261.84	1417.59
	Heat (kW)	66.55	66.55	126.49	170.72	170.72
	RIES (kW)	137.62	1088.4	1432.81	1636.97	1944.72
Scheme 3	Electricity (kW)	87.22	245.51	245.51	411.50	563.61
	Gas (kW)	0.00	817.44	1101.91	1261.84	1417.59
	Heat (kW)	86.16	90.21	171.54	231.91	231.91
	RIES (kW)	173.38	1153.16	1518.96	1905.25	2213.11
Scheme 4	Electricity (kW)	79.85	204.41	204.41	204.41	356.41
	Gas (kW)	68.41	1034.17	1469.03	1469.03	1469.03
	Heat (kW)	80.50	80.50	153.00	206.50	206.50
	RIES (kW)	228.76	1319.08	1826.44	1879.94	2031.94
Scheme 5	Electricity (kW)	75.91	204.41	204.41	204.41	356.41
	Gas (kW)	0.00	817.44	1101.91	1261.84	1417.59
	Heat (kW)	90.21	126.41	126.41	273.66	313.91
	RIES (kW)	166.12	1148.26	1432.73	1739.91	2087.91
Scheme 6	Electricity (kW)	120.55	245.51	245.51	411.50	563.61
	Gas (kW)	168.04	1034.17	1469.03	1469.03	1469.03
	Heat (kW)	105.34	165.46	165.46	210.42	250.35
	RIES (kW)	393.93	1445.14	1880	2090.95	2282.99

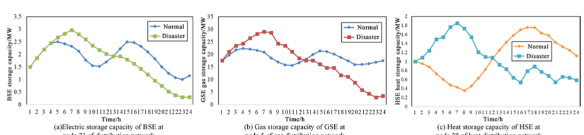

Fig. 5 Energy storage curves of RIES subsystems under different scenarios

CHP2 connected at node 14 further converts the gas energy into electrical energy to meet the higher priority electrical loads at the distribution grid nodes 14, 15 and 17.

In addition, taking the disaster intensity $l=3$ and the disaster occurrence time $t=8$ as an example, the changes of energy storages in each subsystem of the RIES in the normal scenario and the disaster scenario in Scheme 2 are compared, and the results are shown in Fig. 5.

In normal scenarios, the energy storage equipment in each subsystem formulates a charging and discharging plan with the goal of alleviating system load fluctuations. In disaster scenarios, assuming that the time of disaster occurrence is known according to the disaster warning information, the energy storage equipment in each subsystem will be charged and discharged with the goal of achieving the maximum energy storage before the disaster arrives. Taking the electrical energy storage at node 8 of the distribution network as an example, it is known that the disaster occurs at $t=8$, and its storage capacity reaches the maximum at $t=7$. When the pipeline P^{e}_{1-2} is out of operation due to failure and the power supply of the distribution network is partially interrupted, the electrical energy stored by the electrical energy storage device before the disaster will be used for power supply of important gas load. At $t=24$, the electrical energy storage releases a total of 2.675 MW of electrical energy. This greatly reduces the total energy supply shortage of the RIES.

To sum up, the model proposed in this paper aims to minimize the energy supply shortage of the RIES. It can make full use of energy storage in the pre-disaster prevention stage. When the energy supply is interrupted after a disaster, the RIES can ensure the energy supply of key loads by optimizing the dispatch of energy storage, and enhance the resilience of the RIES in disasters.

5.3.4 Sensitivity analysis

Section 5.3.2 has analyzed the resilience level of the RIES under a certain disaster intensity and the hardening strategy of lines/pipelines. This section analyzes the RIES energy supply shortage under Schemes 1 and 2, when the disaster intensity rises from 1 to 5 and the number of lines/pipelines is between 1 and 10. The simulation results are shown in Fig. 6.

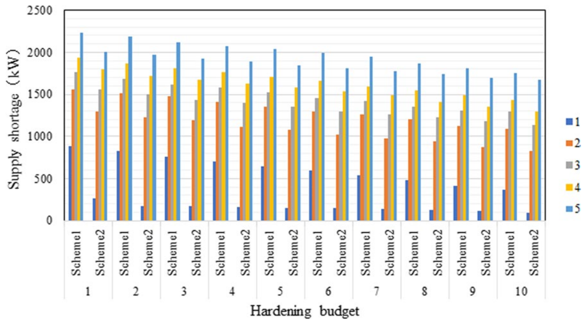

Fig. 6 Energy supply shortages under different hardening budgets and disaster intensities

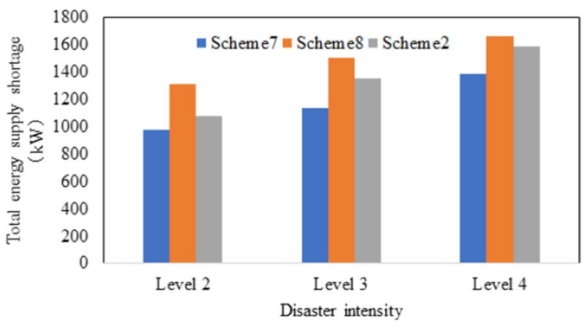

Fig. 7 Energy supply shortages under different failure probabilities and disaster intensities

Under the two schemes, the energy supply shortages decrease with the increase of the number of hardening lines/pipelines, but increase with the increase of disaster intensity. In the case of the same hardening budget and disaster intensity, the total energy supply shortage of Scheme 2 is significantly lower than that of Scheme 1. This proves the effectiveness of the model established in this paper. It is conducive to helping RIES decision-makers evaluate the possible energy supply shortage in the actual disaster situation, so as to develop a more flexible and effective line/pipeline hardening scheme. It can improve the resilience of the RIES in dealing with extreme disaster events of different intensities.

In addition, the total number of fixed lines/pipelines is 6. On the basis of Scheme 2, two different schemes are added, and sensitivity analysis of the two parameters of line/pipeline failure probability and disaster intensity in the three schemes is carried out:

(1) *Scheme 7* Regardless of the different failure probability of each energy subsystem element, set the failure probability of all lines/pipelines to 0.1
(2) *Scheme 8* Regardless of the different failure probability of each energy subsystem element, set the failure probability of all lines/pipelines to 0.3

On the basis of the above schemes, taking the disaster intensity as levels 2–4, the RIES energy supply shortages and hardening strategies in the three schemes are calculated, and the results are shown in Fig. 7 and Table 7.

Combining Fig. 7 and Table 7, the following conclusions can be drawn:

(1) Since the respective set average failure probability of elements in Schemes 7 and 8 is smaller and larger than that in Scheme 2, the respective total energy supply shortage calculated in Schemes 7 and 8 is also smaller and larger than that in Scheme 2. It can be concluded that the different failure probability of each subsystem element of the RIES in disasters has a direct impact on the energy supply shortage of the RIES. If the failure probability is inaccurate, it will not be conducive to judging the actual impact of disasters on the RIES.
(2) As the failure probability of all elements of the RIES is set as a fixed value in Schemes 7 and 8, the elements of the three subsystems have the same priority in the formulation of hardening strategy, and the same number of elements will be hardened. As Scheme 2 takes into account the different failure probability of each subsystem element, and therefore, the elements that are more likely to fail will be hardened preferentially in the formulation of hardening strategies corresponding to different disaster

Table 7 Hardening strategies corresponding to different failure probabilities and disaster intensities

Disaster intensity	Scheme		
	7	**8**	**2**
Level 2	$L^e_{1-2}, L^e_{6-26}, L^g_{1-2}, P^g_{8-9}, L^h_{2-4}, L^h_{14-15}$	$L^e_{1-2}, L^e_{6-7}, P^g_{1-2}, P^g_{8-9}, L^h_{2-4}, L^h_{14-15}$	$L^e_{1-2}, P^e_{6-7}, L^e_{27-28}, L^e_{28-29}, L^g_{8-9}, L^h_{28-31}$
Level 3			$L^e_{1-2}, P^e_{6-7}, L^e_{27-28}, P^g_{8-9}, L^h_{11-13}, L^h_{14-15}$
Level 4		$L^e_{1-2}, L^e_{6-7}, P^g_{8-9}, P^g_{9-10}, L^h_{2-4}, L^h_{14-15}$	$L^e_{1-2}, L^e_{6-7}, P^g_{8-9}, P^g_{9-10}, L^h_{11-13} L^h_{14-15}$

intensities. For example, when the disaster intensity is level 2, the average failure probabilities of the elements of the electrical, gas and heat subsystems are 0.3, 0.05 and 0.08, respectively. Therefore, the elements of the electrical subsystem will be hardened preferentially to minimize the possible energy shortage caused by the disaster.

(3) In conclusion, the RIES hardening strategies obtained at different element failure probability settings are different. Therefore, the integration of accurate element failure information has an important reference significance for the formulation of RIES resilience promotion strategies.

6 Conclusion

This paper studies the resilience improvement technology of an RIES in the pre-disaster prevention and disaster resistance integration stages, and establishes a hardening model of the RIES based on three-layer robust optimization. The upper-layer model decides the best hardening strategy for lines/pipelines, while the middle-layer model considers the different failure probabilities of power lines, gas and heating pipelines, and determines the failure events that can cause the maximum resilience loss of the RIES at a specific disaster intensity. The lower-layer model minimizes the total energy shortage of the RIES by optimizing its operation according to the hardening strategy and fault events. The effectiveness of the proposed hardening model and CCG algorithm is verified by case analysis, and the following conclusions are drawn:

(1) The hardening model of an RIES based on the three-layer robust optimization proposed in this paper makes hardening strategies for improving resilience according to different disaster intensities.

(2) The traditional *N*–*K* criterion does not consider the failure probability of lines and pipelines in disasters, and only determines the hardening strategy by identifying the fault conditions that can cause the greatest energy supply shortage. In contrast, the model proposed in this paper considers different failure probabilities of elements in the decision-making process, i.e., buried pipelines have lower failure probabilities than overhead lines in disasters. Thus, the calculation results are more in line with the actual situation.

(3) As the link of RIES integration and key emergency response resource, energy storage and its optimized operation provide the RIES with resistance to disasters. They enhance the resilience of the system and provide an important guarantee for safe and economical operation.

Since the research in this paper is aimed at the integration stage of pre-disaster prevention and disaster resistance, the assumption that "once a line or pipeline is damaged, it will be out of operation" is made at the modeling stage. When the fault elements are out of operation, the energy supply capacity and efficiency of the RIES decrease, and the energy supply shortage increases, leading to the decrease of the resilience of the RIES. However, in the post-disaster recovery phase, if the RIES fault repair and energy supply recovery plans are designed to shorten the recovery time, the energy supply shortage of the RIES can be reduced and the resilience can be improved. Therefore, to improve the resilience, it is also important to repair the faulty elements in time and restore energy supply quickly. Subsequent research will focus on fault repair and energy supply recovery to improve resilience in the disaster response and post-disaster recovery phases.

Appendix 1

See Figs. 8, 9, 10 and 11.

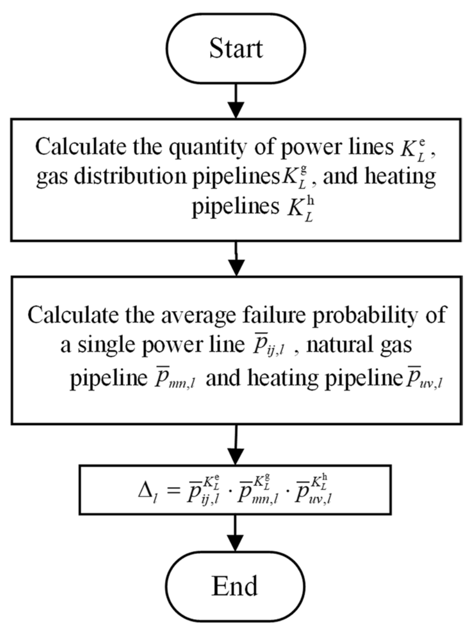

Fig. 8 Δ_l calculation process

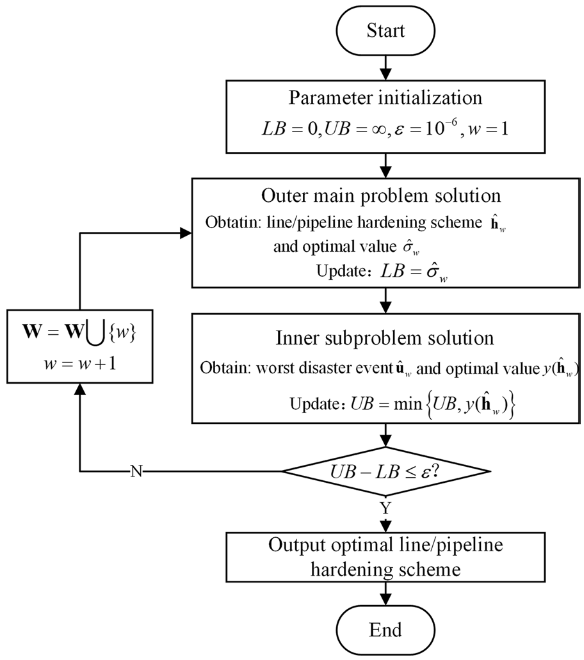

Fig. 9 Solution flow of the three-level robust optimization model for the enhancement of RIES, where $y(\cdot)$ is the objective function of the inner subproblem

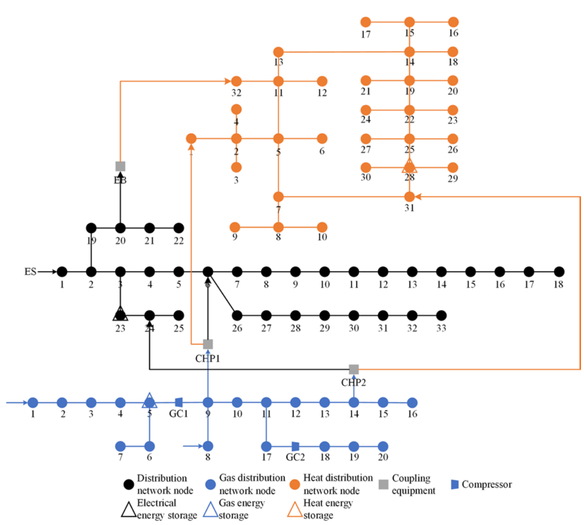

Fig. 10 Structure of the RIES

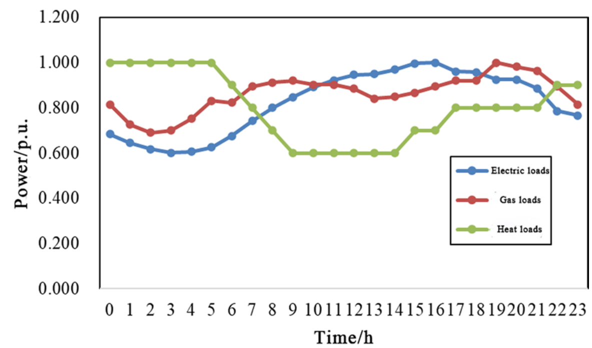

Fig. 11 Electrical/natural gas/heat load profiles on a typical day

See Tables 8, 9 and 10.
Assumptions;

(1) Once lines/pipelines are damaged, the system cannot be used until it enters the repair phase.
(2) Hardened distribution lines, gas and heating pipelines can withstand natural disasters.
(3) This paper focuses on network hardening, and elements such as CHP, EB, compressors, and energy storage are generally more resilient than lines/pipelines. Therefore, they are not considered to be affected by disasters for the time being, and can be used to improve the operating state of the RIES when disasters permeate.
(4) In this paper, it is assumed that DG will be out of operation because of a fault in the disaster, and the operating state of the system will be improved by optimizing the charging and discharging plan of various types of energy storage.
(5) Electrical/gas energy storage can only supply energy to loads connected to the same node or its child nodes.

Table 8 Parameters of energy storage equipment in the RIES test system

Energy storage	Charging efficiency	Energy release efficiency	Rated capacity (MWh)	Rated power (MW)	Initial energy (MW)	Access node
Electrical energy storage	0.9	0.9	3	1.5	1.5	Distribution network node 23
Gas energy storage	0.95	0.95	60	17.59	17.59	Distribution network node 28
Heat energy storage	0.85	0.85	2	1	1	Distribution network node 5

Table 10 Node priority weights of the RIES test system

Node weight	Weight coefficient	Distribution network node	Gas distribution network node	Heat distribution network node
1	0.1	12, 16, 19, 21, 25, 30, 32	2, 12	13, 16–18, 20–21
2	0.3	3–4, 9, 20, 23, 27, 33	3, 4, 11, 19	3–6, 8–10, 12, 23–24, 26–27, 29–30
3	0.7	5–6, 10, 18, 24, 29, 31	7, 16–17	14–15, 19, 22, 25, 28
4	0.9	7–8, 11, 14, 17, 22, 26, 28	13–15, 20	2, 7, 11
5	1.0	2, 13, 15	6, 10	1, 31–32

Table 9 Equipment parameters of the CHP

Equipment	Upper limit of electric power supply/consumption (MW)	Upper limit of heat power supply (MW)	Upper limit of natural gas supply/consumption (MW)	Water supply temperature (℃)
CHP1	0.8	1.04	2	70
CHP2	0.8	1.04	2	70
EB	0.5	0.75	–	70

Abbreviations

IES	Integrated energy system
RIES	Regional integrated energy system
GT	Gas turbine
GB	Gas boiler
EB	Electric boiler
CHP	Combined heat and power
SOE	State of energy
CCG	Column-and-constraint generation
MILP	Mixed integer linear programming
GS	Gas source

Authors' information

Jiaqing Wu, Major in the AI-related applications in integrated energy system and power system oscillation.
Jie Gu, PHD and Associate Professor at Shanghai Jiao Tong University, Major in power system planning, power markets, smart grids, microgrids, and intelligent algorithms.
Shuqi Liu, M.S, Major in the power system planning and integrated energy system.
Zhijian Jin, PHD and professor at Shanghai Jiao Tong University, research interests include application of high temperature superconductivity, energy Internet, and online detection technology of power equipment.

Acknowledgements
I would like to show my gratitude to Department of Electrical Engineering, Shanghai Jiao Tong University for providing necessary facilities to carry out the work.

Author contributions
Demand research, literature survey, experiment design, data collection, mathematical modeling, case study, and paper writing. All authors read and approved the final manuscript.

Funding
This work was supported in part by Key Project of Shanghai Science and Technology Committee (18DZ1100303).

Availability of data and materials
The datasets used and analyzed during the current study are available from the corresponding author on reasonable request.

Declarations

Competing interests
The authors declare that they have no known competing financial interests or personal relationships that could have appeared to influence the work reported in this paper.

Received: 6 September 2022 Accepted: 15 May 2023
Published online: 03 July 2023

References

1. Lin, Y., & Bie, Z. (2016). Study on the resilience of the integrated energy system. *Energy Procedia, 103*, 171–176.
2. Li, X., Sun, T., Hou, K., et al. (2020). Evaluating resilience of island integrated energy systems with earthquake. *Proceedings of the CSEE, 40*(17), 5476–5493.
3. Mousavizadeh, S., Alahyari, A., Ghodsinya, S. R. M., et al. (2021). Incorporating microgrids coupling with utilization of flexible switching to enhance self-healing ability of electric distribution systems. *Protection and Control of Modern Power Systems, 6*(1), 1–11.
4. Panteli, M., & Mancarella, P. (2015). Modeling and evaluating the resilience of critical electrical power infrastructure to extreme weather events. *IEEE Systems Journal, 11*(3), 1733–1742.
5. Salman, A., Li, Y., & Stewart, M. (2015). Evaluating system reliability and targeted hardening strategies of power distribution systems subjected to hurricanes. *Reliability Engineering & System Safety, 144*, 319–333.
6. Yuan, W., Wang, J., Qiu, F., et al. (2016). Robust optimization-based resilient distribution network planning against natural disasters. *IEEE Transactions on Smart Grid, 7*(6), 2817–2826.
7. Ma, S., Chen, B., & Wang, Z. (2016). Resilience enhancement strategy for distribution systems under extreme weather events. *IEEE Transactions on Smart Grid, 9*(2), 1442–1451.
8. Qi, S., Wang, X., Shao, C., et al. (2019). Resilience analysis of integrated electricity and natural gas energy system under extreme events. *Power System Technology, 43*(1), 41–51.
9. Shao, C., Shahidehpour, M., Wang, X., et al. (2017). Integrated planning of electricity and natural gas transportation systems for enhancing the power grid resilience. *IEEE Transactions on Power Systems, 32*(6), 4418–4429.

10. Aldarajee, A., Hosseinian, S., Vahidi, B., et al. (2020). A coordinated planner-disaster-risk-averse-planner investment model for enhancing the resilience of integrated electric power and natural gas networks. *International Journal of Electrical Power & Energy Systems, 119*, 105948.
11. Wu, K., Gu, J., Meng, L., et al. (2022). An explainable framework for load forecasting of a regional integrated energy system based on coupled features and multi-task learning. *Protection and Control of Modern Power Systems, 7*(1), 1–14.
12. Lu, Y., Li, H., Liu, Y., et al. (2022). Optimal operation of electricity-gas-heat integrated energy system considering therisk of energy supply equipment failure. *Power System Protection and Control, 50*(9), 34–44.
13. Shen, Y., Gu, C., Ma, Z., et al. (2021). A two-stage resilience enhancement for distribution systems under hurricane attacks. *IEEE Systems Journal, 15*, 653–661.
14. Yu, Z., Zou, G., Wu, L., et al. (2021). Optimal resilience enhancement strategy for power distribution system with line reinforcement and emergency generator placement. In: *IEEE Sustainable Power and Energy Conference*, pp. 1400–1405.
15. Canham, C., Papaik, M., & Latty, E. (2001). Interspecific variation in susceptibility to windthrow as a function of tree size and storm severity for northern temperate tree species. *Canadian Journal of Forest Research, 31*(1), 1–10.
16. Xu, X., Jia, H., Jin, X., et al. (2015). Study on hybrid heat-gas-power flow algorithm for integrated community energy system. *Proceedings of the CSEE, 35*(14), 3634–3642.
17. Li, Z., Han, A., Zhou, S., et al. (2021). Optimization of an integrated energy system considering integrated demand response. *Power System Protection and Control, 49*(21), 36–43.
18. Diao, H., Li, P., Wang, J., et al. (2020). Optimal dispatch of integrated energy system considering complementary coordination of electric/thermal energy storage. *Transactions of China Electro Technical Society, 35*(21), 4532–4543.
19. He, C., Dai, C., Wu, L., et al. (2018). Robust network hardening strategy for enhancing resilience of integrated electricity and natural gas distribution systems against natural disasters. *IEEE Transactions on Power Systems, 33*(5), 5787–5798.
20. Wang, C., Bie, Z., Pan, C., et al. (2019). Contingency intelligent screening and ranking approach for integrated energy system considering expected loss. *Power System Technology, 43*(21), 44–53.

Submit your manuscript to a SpringerOpen journal and benefit from:

- ► Convenient online submission
- ► Rigorous peer review
- ► Open access: articles freely available online
- ► High visibility within the field
- ► Retaining the copyright to your article

Submit your next manuscript at ► springeropen.com